

An Approximation for the Capture Radius of Gaseous Protoplanets

Claudio Valletta,¹* Ravit Helled,¹

¹Center for Theoretical Astrophysics & Cosmology, Institute for Computational Science, University of Zurich, Zurich, Switzerland

Accepted 2021 July 23. Received 2021 July 19; in original form 2021 June 10

Key words: methods: numerical — planets and satellites: formation, gaseous planets — protoplanetary disks – planet-disk interactions

ABSTRACT

Determining the heavy-element accretion rate of growing giant planets is crucial for understanding their formation and bulk composition. The solid (heavy-element) accretion rate should be carefully modeled during the various stages of giant planet formation and therefore, the planetary capture radius must be determined. In some simulations that model the heavy-element accretion rate, such as in N-body simulations, the presence of the gaseous envelope is either neglected, or treated in an over-simplified manner. In this paper, we present an approximation for the capture radius that does not require the numerical solution of the stellar structure equations. Our approximation for the capture radius works extremely well for various planetesimal sizes and compositions. We show that the commonly assumed constant density assumption for inferring the capture radius leads to a large error in the calculated capture radius and we therefore suggest that our approximation should be implemented in future simulations.

1 INTRODUCTION

In the *core accretion* model (Pollack et al. 1996), the standard model for giant planet formation, the growth of a giant planet begins with the formation of a heavy-element core (Helled et al. 2014). Once the core reaches about Mars’ mass, its gravity is sufficiently high to accrete hydrogen and helium (hereafter, H-He) gas from the proto-planetary disk. The proto-planet continues growing by accreting both solids (heavy elements), in the form of planetesimals (0.1 - 100 km sized objects), and H-He until the so-called crossover mass is reached (Lissauer et al. 2009; Ginzburg & Chiang 2019) and runaway gas accretion takes place. In this last stage the planet detaches from the disk and collapses under the influence of its gravity.

The heavy-element accretion rate can be modeled using Safronov’s equation (Safronov 1969), which is a useful approximation for the accretion of the surrounding planetesimals onto a planetary embryo:

$$\frac{dM_{\text{solid}}}{dt} = \dot{M}_{\text{core}} = \pi R_{\text{capt}}^2 \sigma_s \Omega F_g, \quad (1)$$

where πR_{capt}^2 is the geometrical capture cross section, where R_{capt} is the capture radius, Ω is the orbital frequency, σ_s is the solid surface density in the disk, and F_g is the gravitational enhancement factor for the cross section with respect to the geometrical value, as computed by Greenzweig & Lissauer (1992). If the proto-planet does not hold a gaseous envelope R_{capt} equals the core’s radius. The presence of the envelope increases the capture radius by orders of magnitude (e.g., Pollack et al. 1996). The solid accretion rate depends on R_{capt}^2 , therefore it is important to have a realistic estimate of the capture radius.

A key goal of giant planet formation theory is to explain the bulk composition of giant planets. In order to predict the planetary composition, the total mass of heavy elements that are captured during the planetary growth must be computed accurately. This is, however, not an easy task because the heavy-element accretion rate depends on two distinct physical aspects: the orbit of the planetesimals disk under the effect of the gravitational force exerted by the planet (Shibata & Ikoma 2019; Shibata et al. 2020) and the interaction between planetesimals and the growing proto-planet (Inaba & Ikoma 2003; Iaroslavitz & Podolak 2007; Brouwers et al. 2018; Valletta & Helled 2019). The former is typically computed using N-body simulations (e.g., Shibata & Ikoma 2019; Podolak et al. 2020), while the planet’s structure is modeled via planetary codes that solve numerically the structure equations (e.g., Valletta & Helled 2020; Vazan et al. 2018; Helled & Bodenheimer 2014).

N-body simulations compute accurately the orbits of planetesimals around the central star and the proto-planet. However, the envelope’s structure and the capture radius are typically modeled in an over-simplistic way. For example, Shibata & Ikoma (2019) simulated the orbits 10,000 of planetesimals including the gravitational presence of the proto-Jupiter, assuming *in-situ* formation, in its late formation stage. They also included the gravitational effect of the proto-planet on the gas disk as well as gap opening. It was found that the mass of planetesimals captured by proto-Jupiter during the gas accretion is $\sim 3 M_{\oplus}$. It was then concluded that a very high solid surface density is required to explain the total heavy-element mass in Jupiter. In Shibata et al. (2020) the same computational method was used to estimate the amount of captured planetesimals when planetary migration is included. It was found that the amount of captured solids increases with increasing migration distances.

However, in both of these recent studies a naive assumption for

* E-mail: claudiovalletta92@gmail.com

the capture radius was used. It was assumed that the capture radius is given by the proto-planetary mass and an a-priori assumed density, following the relation $M = 4/3\pi\rho R_{\text{capt}}^3$, where R_{capt} , ρ and M are the capture radius, the planet's density and planet's mass, respectively. This is a rough approximation because while the planet is forming and gas is accreted the proto-planet density changes significantly. This can have important consequences on R_{capt} .

In order to predict correctly the capture radius one should compute the trajectory of the planetesimals, solve the stellar structure equations within the proto-planet's envelope and take into account the drag force that the atmosphere exerts on the planetesimals. Inaba & Ikoma (2003) derived an approximate expression for the capture radii of proto-planets. They showed that R_{capt} is significantly larger than the core's radius and that it mostly depends on the planetesimal's size, where R_{capt} is larger for smaller planetesimals. However, their expression for R_{capt} requires the knowledge of how the density change within the planet's envelope, i.e. it requires the numerical solution of the structure equation within the proto-planet. Therefore the formulation by Inaba & Ikoma (2003) can not be implemented in works similar to Shibata & Ikoma (2019).

In this paper, we derive an approximation for R_{capt} that does not require a numerical solution of the structure equations. This approximation is valid throughout the entire planetary growth: when the planet is attached to the disk, and when it is detached from the disk and runaway gas accretion takes place. The approximation presented here is useful for models that do not directly compute the structure of the planetary envelope, such as N-body simulations. In addition, using this approximation would significantly improve the prediction of the heavy-element accretion rate in comparison to calculations where the planet is assumed to have a constant density.

2 METHODS

2.1 The attached phase

Initially, the proto-planet is attached to the disk and the outer pressure, temperature and density are determined by its orbital location. Following Lissauer et al. (2009) we define the planet's outer radius as:

$$R_0 = \frac{GM_P}{c_s^2 + \frac{GM_P}{0.25R_H}}, \quad (2)$$

where M_P is the planet's mass, c_s is the sound speed in the disk and R_H is the Hill's radius. In this early phase, the gas accretion rate is obtained by demanding that the computed radius of the planet is equal to Eq. 2. The structure equations of mass conservation, hydrostatic balance, thermal gradients, and energy conservation that regulate the envelope's structure are given by:

$$\begin{aligned} \frac{dm}{dr} &= 4\pi r^2 \rho \\ \frac{dP}{dr} &= -\frac{Gm}{r^2} \rho \\ \frac{dT}{dr} &= \nabla \frac{T}{P} \frac{dP}{dr} \\ \frac{dL}{dr} &= 4\pi r^2 \rho \left(\epsilon - T \frac{\partial S}{\partial t} \right), \end{aligned} \quad (3)$$

where m and r are the mass and radius coordinates, ρ , P and T are the density, pressure, and temperature within the envelope, L and S are the luminosity and the entropy and the third equation defines the temperature gradient $\nabla \equiv d \ln t / d \ln P$. We denote the

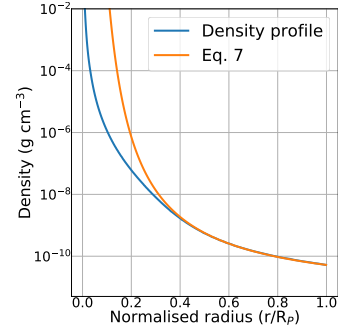


Figure 1. Density as a function of the normalised radius (r/R_P) within the proto-planet's envelope. The blue and orange lines correspond to the density obtained numerically and using our approximation, respectively. The orbital location is assumed to be 5.2 AU and the total mass of the planet is $20 M_{\oplus}$.

outermost pressure, temperature, and density by P_0 , T_0 and ρ_0 . The approximation of the capture radius depends on these values, which are parameters in our formula. To provide a comparison with the numerical computation we follow Piso et al. (2015) to compute their value.

The capture radius is determined by the gas drag exerted on the planetesimals, which is affected by the density profile within the envelope. Therefore, in order to estimate R_{capt} the density profile of the atmosphere needs to be determined. In particular, is important to have a good approximation for the density profile in the outer layers that have a larger influence on the planetesimal's orbit in comparison to the deep interior. We therefore focus on inferring the density profile in the outer regions of the planet.

As shown by various studies, radiation transports the heat in the outer layers of the proto-planet (Piso et al. 2015; Brouwers & Ormel 2020). In this zone the temperature is nearly constant, while the pressure and density increase exponentially towards the planetary center. We can therefore represent the temperature, pressure, and density of the envelope by:

$$\begin{aligned} T(r) &= T_0 \\ P(r) &= P_0 \exp\left(\alpha(R_0/r - 1)\right) \\ \rho(r) &= \rho_0 \exp\left(\alpha(R_0/r - 1)\right) \end{aligned} \quad (4)$$

Substituting Eq.4 in the second equation of Eq.3 leads to:

$$\alpha = \frac{GM\rho_0}{P_0R_0}, \quad (5)$$

where we assume that the mass coordinate m is equal to the total mass of the planet M , which is a good assumption in the outer layers of the planet. The density is therefore given by:

$$\rho(r) = \rho_0 \exp\left(\alpha(R_0/r - 1)\right). \quad (6)$$

Figure 1 shows the comparison between Eq. 6 and the density obtained by solving numerically the planetary structure equations. All the numerical solutions presented in this paper are obtained using the updated model for giant planet formation presented in Valletta & Helled (2020). It can be seen that in a large part of the envelope the result is extremely good. Near the planet's center, the ansatz used to derive Eq. 6 is no longer valid because the behavior of the density is not exponential. The Eq. 6 could be included in N-body

simulations to include the presence of the planetary envelope in the equation of motion of planetesimals. In Appendix A we show further comparisons for various planetary masses and orbital locations.

We can use Eq. 6 to derive an approximation for the capture radius. Inserting Eq. 6 in equation 18 of Inaba & Ikoma (2003) we find that:

$$R_{\text{capt}} = \frac{R_0}{1 + \frac{1}{\alpha} \ln\left(\frac{\rho_\star}{\rho_0}\right)}, \quad (7)$$

where

$$\rho_\star = \frac{2r_p\rho_p}{3DR_H}, \quad (8)$$

and r_p and ρ_p are the planetesimal's size and density, respectively. D represents the drag coefficient defined in Eq. 11 of Inaba & Ikoma (2003). The drag coefficient is computed according to Podolak et al. (1988) and for our conditions D is close to unity, and therefore we use $D = 1$ in the calculation. In principle, the value of R_{capt} also depends on the initial velocity of the planetesimals. In Equation 7 it is assumed that the initial planetesimal velocity is much smaller than the escape velocity from the protoplanet. We find that the initial velocity has almost no effect on the capture radius. In order to derive an approximation for R_{capt} considering different initial velocities it is sufficient to insert Equation 6 in Equation 17 of Inaba & Ikoma (2003). However, in this case there is no longer an analytic solution for R_{capt} .

In Appendix B we investigate the sensitivity of our results to the assumed planetesimal's composition. Figure 2 shows a comparison between Eq. 7 (solid-line) and R_{capt} computed numerically with the formula of Inaba & Ikoma (2003) (dashed-line). We find that for small planetesimals our approximation is excellent, while the agreement is less good when assuming large planetesimals. However, the difference is typically within a factor of two. The brown line indicates the constant density approximation used in Shibata & Ikoma (2019). There are orders of magnitude of difference between this assumption and the numerical result. In the right panel of Fig. 2 we show the planet's mass as a function of time, when accreting 100-km-sized planetesimals. We use the heavy-element accretion rate of Pollack et al. (1996). The solid accretion rates depends on R_{capt}^2 . It is clear from the figure that using the constant density approximation leads to unrealistic estimates of the capture radius (by orders of magnitude), which in turn affects the planetary growth and therefore should not be applied.

2.2 The detached phase

When the gas accretion rate is limited by the maximum that the disk can supply (Lissauer et al. 2009) the proto-planet detaches from the disk, and as a result, the approximation derived in Equation 7 is no longer appropriate. We assume that the detached phase begins at the crossover mass, i.e. when the total mass of heavy-element equals the total mass of H-He (Brouwers & Ormel 2020). In this phase the radius collapses very rapidly and then slowly decreases over time. After the planet reaches the point at which $M_Z = M_{H-He}$, R_{capt} can be approximated as constant. We show in Appendix C that the radius does not depend on the runaway gas accretion rate. Instead, it depends on the ratio between the total mass of heavy-elements and the mass of H-He. The left panel of Fig. 3 shows the planet's radius for different values of M_Z/M_{H-He} . Each triangle and dot indicate the value of the radius after 10^7 and 10^8 years from the beginning of the simulation, respectively. The different colors represent different orbital locations. The black lines correspond to our fit. The planet's

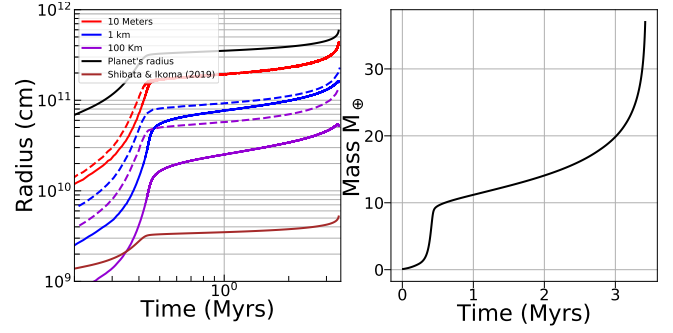


Figure 2. Left: R_{capt} vs. time for various planetesimal sizes. The blue, brown, and purple curves correspond to planetesimal sizes of 10 meters, 1 km, and 100 km, respectively. The solid line indicates our Eq. 6, while the dashed line corresponds to R_{capt} calculated using the approximation of Inaba & Ikoma (2003) and using the numerical solution for the density profile. Finally, the brown line represents the commonly used constant-density assumption Shibata & Ikoma (2019). **Right:** Planetary mass vs. time assuming the planet is growing by accreting 100-km-sized planetesimals.

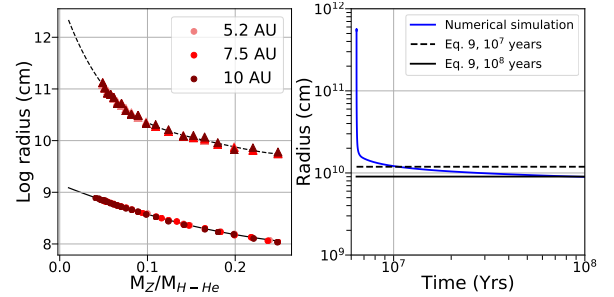


Figure 3. Left: Planet's radius as a function of M_Z/M_{H-He} . Each triangle and dot represent the radius of the planet after 10^7 and 10^8 years from its formation, respectively. Different colours represent different orbital locations. **Right:** The planet's radius computed numerically (blue-line) and Eq. 9 (black-line) as a function of time.

radius decreases with increasing M_Z/M_{H-He} and decreases with time. We find that there is no difference between the various colours, and we therefore conclude that the value of the radius is independent of the assumed orbital location. It should be noted, however, that we have neglected the radiation from the star. This can have important effects for close-in giant planets ($< 0.5\text{AU}$) and we hope to include this effect in future research.

The fit corresponding to Figure 3 is given by

$$R = \left(\sum_{i=0}^4 R_i \frac{M_Z^i}{M_{H-He}^i} \right) \times 10^9 \text{ cm}, \quad (9)$$

where $R_0 = 12.80662188$, 9.15426162 , $R_1 = -50.86303789$, -6.74548399 , $R_2 = 382.66267044$, 9.40271959 , $R_3 = -1388.57741163$, 0 and $R_4 = 1902.60362959$, 0 . The former and latter values of the coefficients correspond to the 10^7 years and to the 10^8 years fit, respectively. Between 10^7 and 10^8 years the radius can be derived with a logarithmic interpolation between these two values. The right panel of Fig. 3 shows the planet's radius vs. time during the detached phase, comparing Eq. 9 with the radius computed numerically. It can be seen that after a short time at which the planet shrinks rapidly, the radius can be approximated as a constant. Eq. 9 is an approximation. The planet's radius depends on several other quantities such as the total planetary mass and the core's

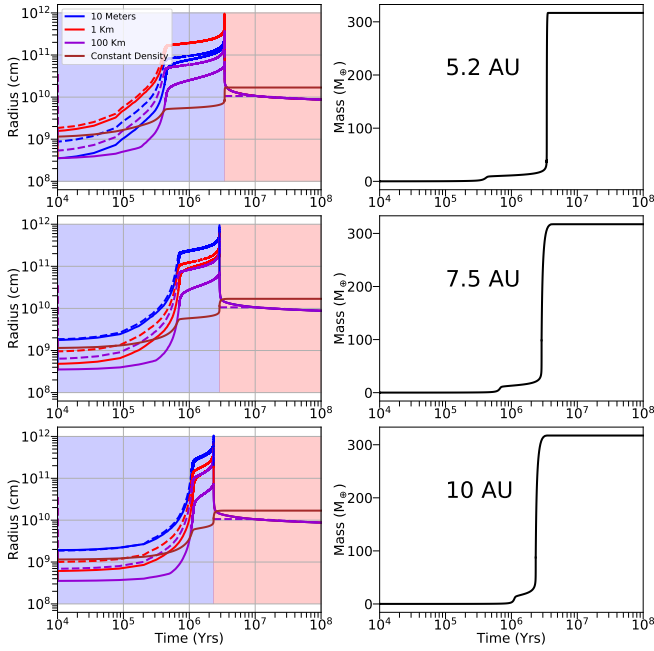


Figure 4. Left: R_{capt} as a function of time for different planetesimal sizes. The blue, red and purple curves correspond to sizes of 10 meters, 1 km and 100 km, respectively. The brown curve represents the constant density approximation used in Shibata & Ikoma (2019). The solid line shows R_{capt} computed with Eq. 18 of Inaba & Ikoma (2003) using the density profile obtained numerically, while the dashed line represents our Eq. 10. The blue and red shaded regions indicate the attached and detached phase, respectively. **Right:** Planetary mass as a function of time. The various lines correspond to different formation locations.

luminosity. However, the dominating property is the ratio between the heavy-element and H-He mass, M_Z/M_{H-He} (e.g., Fortney et al. 2007; Baraffe, I. et al. 2008).

RESULTS

In this section we present the results for the entire planetary growth. We suggest that R_{capt} should be approximated as follows:

$$R_{\text{capt}} = \begin{cases} \frac{R_0}{1 + \frac{1}{\alpha} \ln\left(\frac{\rho_*}{\rho_0}\right)} & \text{if } M_Z > M_{H-He}, \\ \text{Eq. 9} & \text{otherwise} \end{cases} \quad (10)$$

Figure 4 presents the comparison between Eq. 10 and R_{capt} computed with Eq. 18 of Inaba & Ikoma (2003) using the density computed numerically with our code (Valletta & Helled 2020). Different dots' colours in the plot indicate different formation locations of 5.2 AU, 7.5 AU, and 10 AU. The right panel plot shows the planet's mass vs. time. We find that during most of the formation timescale there is a very good agreement between Eq. 10 and the numerical results. In particular, during the detached phase there is a small difference between the two results. When the planet is attached to the disk the approximation is extremely accurate for small and intermediate-size planetesimals (size ≤ 1 km), while for large planetesimals there is a difference of \sim a factor of two. However, it can be seen that for all the planetesimal sizes the result is more accurate than the constant density approximation which is often used in formation models.

3 SUMMARY & CONCLUSIONS

In order to have robust theoretical predictions for the bulk composition of giant planets, the heavy-element mass accreted during the planetary formation should be estimated. A key parameter in determining the heavy-element mass in growing giant planets is the capture radius. The presence of the gas increases significantly the capture radius and as N-body simulations typically do not account for the planetary structure it is important to find an appropriate approximation for R_{capt} accounting for the gaseous envelope.

In this study we present an approximation for R_{capt} which is valid throughout the different stages of the planetary growth and can easily be implemented in N-body simulations. This approximation does not require the solution of the stellar structure equations. It can be used to track consistently the formation of a giant planet in an N-body code, modeling the change in the capture radius as more and more gas is accreted. This can not be done when assuming that the planet's density remains constant because the accretion of gas decreases significantly the planet density by increasing its radius. We divide the planetary formation into two phases: (1) when the planet is attached to the disk ($M_Z > M_{H-He}$), and (2) when the planet detaches from the disk ($M_{H-He} > M_Z$). We compare our approximation with numerical results and find that the approximation is working extremely well and suggest that this approximation should be implemented in giant planet formation models in order to correctly infer the heavy-element accretion rate of growing giant planets.

ACKNOWLEDGEMENTS

The authors acknowledge support from SNSF grant 200020_188460 and the National Centre for Competence in Research 'PlanetS' supported by SNSF.

DATA AVAILABILITY

The data underlying this article will be shared on reasonable request to the corresponding author.

REFERENCES

- Baraffe, I. Chabrier, G. Barman, T. 2008, *A&A*, 482, 315
Brouwers M. G., Ormel C. W., 2020, *A&A*, 634
Brouwers Vazan, A. Ormel, C. W. 2018, *A&A*, 611, A65
Fortney J. J., Marley M. S., Barnes J. W., 2007, *The Astrophysical Journal*, 659, 1661
Ginzburg S., Chiang E., 2019, *Monthly Notices of the Royal Astronomical Society*, 487, 681
Greenzweig Y., Lissauer J. J., 1992, *Icarus*, 100, 440
Helled R., Bodenheimer P., 2014, *The Astrophysical Journal*, 789, 69
Helled R., et al., 2014, in Beuther H., Klessen R. S., Dullemond C. P., Henning T., eds, *Protostars and Planets VI*. p. 643 ([arXiv:1311.1142](https://arxiv.org/abs/1311.1142)), [doi:10.2458/azu_uapress_9780816531240-ch028](https://doi.org/10.2458/azu_uapress_9780816531240-ch028)
Iaroslavtsev E., Podolak M., 2007, *Icarus*, 187, 600
Inaba S., Ikoma M., 2003, *A&A*, 410, 711
Lissauer J. J., Hubickyj O., D'Angelo G., Bodenheimer P., 2009, *Icarus*, 199, 338
Piso A.-M. A., Youdin A. N., Murray-Clay R. A., 2015, *ApJ*, 800, 82
Podolak M., Pollack J. B., Reynolds R. T., 1988, *Icarus*, 73, 163
Podolak M., Haghighipour N., Bodenheimer P., Helled R., Podolak E., 2020, *ApJ*, 899, 45
Pollack J. B., Hubickyj O., Bodenheimer P., Lissauer J. J., Greenzweig Y., 1996, *Icarus*, 124, 62
Safronov V. S., 1969, *NASA Tech. Trans.*, pp F-677

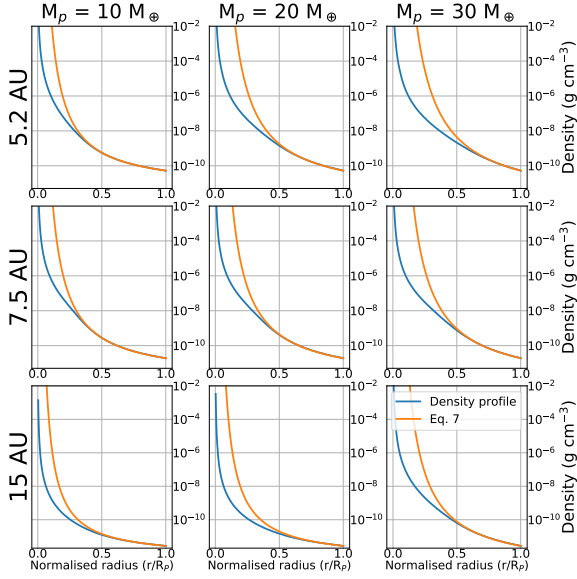


Figure A1. Density as a function of the normalised radius r/R_p . The blue line represents the numerical result, while the orange line corresponds to Eq. 6. Different lines in the figure represent different orbital locations, while different columns indicate different total planetary masses.

Shibata S., Ikoma M., 2019, *Monthly Notices of the Royal Astronomical Society*, 487, 4510

Shibata Helled Ikoma 2020, *A&A*, 633, A33

Valletta Helled 2019, *The Astrophysical Journal*, 871, 127

Valletta C., Helled R., 2020, *The Astrophysical Journal*, 900, 133

Vazan Helled Guillot 2018, *A&A*, 610, L14

APPENDIX A: AN APPROXIMATION FOR THE DENSITY PROFILE OF THE ENVELOPE

In this section we present further comparisons between Eq. 6 and the density profile computed numerically. In Fig A1 the blue line indicates the density profile computed numerically, while the orange line represents Eq. 6. Different lines represent different orbital’s locations, while different columns represent different total planetary masses. In all the cases there is an excellent agreement between the two results in the outer \sim half of the planet, while for normalised radius less than 0.5 the two lines are very different. In this region the ansatz used to derive Eq. 6 is not valid.

APPENDIX B: DEPENDENCE OF R_{capt} ON THE PLANETESIMAL’S COMPOSITION

All the results presented above correspond to icy planetesimals with a density of 1 g cm^{-3} . Clearly, it is also important to investigate how R_{capt} changes with the assumed planetesimal’s composition. The planetesimal’s density affects the capture radius via the drag force exerted by the envelope’s gas on the planetesimal.

The sensitivity of R_{capt} on the planetesimal’s composition is shown in Figure B1. The left and right panels show the results when assuming planetesimal sizes of 1 km and 100 km, respectively. We compare the inferred R_{capt} for planetesimals composed of pure-rock and pure-water. Rock is represented by SiO_2 , with a material density of 2.7 g cm^{-3} . The solid lines indicate the result of Inaba & Ikoma (2003) using the density profile obtained numerically, while the dashed ones represent our Eq. 7. As expected, planetesimals of

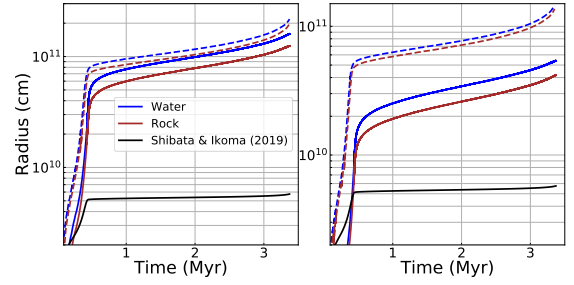


Figure B1. R_{capt} as a function of time. In the left and right panel plot the planetesimal’s size is assumed to be 1 km and 100 km, respectively. Different colours represent different planetesimal compositions where the blue and brown lines correspond to planetesimals made of water and rock, respectively. The solid lines correspond to the result of Inaba & Ikoma (2003) while the dashed ones correspond to Eq. 7.

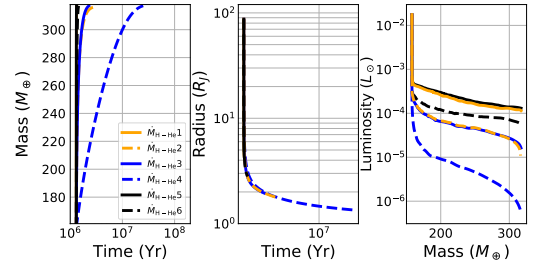


Figure C1. Left: Planetary mass as a function of time for different runaway gas accretion rates. **Middle:** Radius of the planet (in Jupiter’s radii units) as a function of time. **Right:** Planetary luminosity as a function of time. The different runaway gas accretion rates are defined in Valletta & Helled (2020)

lower (higher) density have a larger (smaller) capture radius. Different assumed planetesimal compositions would slightly affect our approximation via the parameter ρ_* introduced in Equation 8, and indeed as shown in Figure B1, R_{capt} depends on the assumed planetesimal’s composition. There is a very good agreement between the full numerical results and our approximation for the different assumed planetesimal’s composition. It can be seen that the difference in R_{capt} between different assumed planetesimal’s composition is significantly smaller in comparison to the typical approximations assuming the same planetesimal composition used by Shibata & Ikoma (2019).

APPENDIX C: DETACHED PHASE

In this section we show that the planetary radius does not depend on the assumed \dot{M}_{xy} . Figure C1 shows the radius for different assumed runaway gas accretion rates. The definition of the different rates can be found in Valletta & Helled (2020). The left panel shows the total planetary mass vs. time. There is a large difference between the different gas accretion rates, and in addition, different gas accretion rates lead to different planetary luminosity, as shown in the right panel. The middle panel plot shows the radius as a function of time: all the different gas accretion rates results in a similar radius. This is similar to what found in Figure 1 of Ginzburg & Chiang (2019).